



OPEN Ethoxychelerythrine as a potential therapeutic strategy targets PI3K/AKT/mTOR induced mitochondrial apoptosis in the treatment of colorectal cancer

Yaqin Meng^{1,3,6}, Yanpo Si^{1,6}, Tao Guo¹✉, Weiwei Zhao²✉, Liping Zhang¹, Ya Wang³, Lianping Wang⁴, Ke Sun⁴ & Shuying Feng⁵✉

Several alkaloids found in the *Zanthoxylum* genus have demonstrated significant anticancer activity. However, the antitumor effects of Ethoxychelerythrine (Eth) have not been previously reported. Cell viability, colony formation, apoptosis and cell cycle analysis, intracellular and reactive oxygen species (ROS), mitochondrial membrane potential (MMP) levels of Eth against SW480 cells were evaluated. Subcutaneously transplanted SW480 cells model was used to determine the effect of Eth on tumor growth in vivo. Inflammation levels, angiogenic factors, pathological observations, quantitative reverse-transcription PCR (qRT-PCR), quantitative proteomics, metabolite profiles and western blotting were conducted. It found that Eth significantly inhibited the proliferation of SW480 and HT29 cells in vitro, with stronger inhibitory activity observed against SW480 cells. Therefore, subsequent studies focused on SW480 cells. In vitro, we observed that Eth arrested the cell cycle at the G0/G1 phase, decreased MMP levels, elevated cellular ROS levels, and induced mitochondrial apoptosis. In vitro, Eth significantly inhibited tumor proliferation and metastasis, and regulated the molecule levels of angiogenesis and inflammatory factors in serum, as well as apoptotic protein in tumor tissues. The serum proteomic revealed that the differential proteins were primarily involved in the PI3K/AKT/mTOR pathway, including laminin β 1 (Lamb1), and type I collagen (Col1a1). Metabolomics showed that many abnormal levels of metabolites regulated by the PI3K/AKT/mTOR pathway were obviously reversed towards normal levels after Eth intervention. The correlation analysis between the two-omics revealed that different proteins in the PI3K/AKT pathway, particularly lactate dehydrogenase B (LDHB) and glutathione synthetase (GSS), can interact with most of different metabolites. In summary, Eth exerts anti-tumour effects by inhibiting the activation of the PI3K/AKT/mTOR pathway, which in turn activates mitochondrial apoptosis. Eth may be considered in the development of drugs for relieving colon cancer patients in the future.

Keywords Ethoxychelerythrine, Colorectal cancer, PI3K/AKT/mTOR, Mitochondrial apoptosis, Proteomics, Metabolomics

Abbreviations

| | |
|------|--------------------------------|
| 5-Fu | 5-Fluorouracil |
| bFGF | Basic fibroblast growth factor |
| CP | Carbamoyl phosphate |
| CPS1 | Carbamoyl phosphate synthase 1 |
| CRC | Colorectal cancer |

¹Department of Pharmacy, Henan University of Chinese Medicine, NO 156 JinshuiEast Road, Zhengzhou 450046, China. ²Department of Integrated Therapy, Fudan University Shanghai Cancer Center, No 270 Dong'An Road, Shanghai 200032, China. ³School of Life Science and Engineering, Lanzhou University of Technology, Lanzhou 730050, China. ⁴Lanzhou Foci Pharmaceutical Co., Ltd, Lanzhou 730050, China. ⁵Medical College, Henan University of Chinese Medicine, NO 156 JinshuiEast Road, Zhengzhou 450046, China. ⁶Yaqin Meng and Yanpo Si contributed equally to this work. ✉email: gt010010@hactcm.edu.cn; sunbrightzww@126.com; fsy@hactcm.edu.cn

| | |
|---------------|--|
| Eth | Ethoxychelerythrine |
| DMSO | Dimethyl sulfoxide |
| H&E | Hematoxylin and eosin |
| HMDB | Human metabolome database |
| IAM | Iodoacetamide |
| IHC | Immunohistochemistry |
| IL-6 | Interleukin 6 |
| KEGG | Kyoto encyclopedia of genes and genomes |
| LC | Liquid chromatography |
| MMP | Mitochondrial membrane potential |
| MPTP | Mitochondrial permeability transition pore |
| MTT | 3-(4, 5-Dimethylthiazol-2-yl)-2, 5-diphenyltetrazolium bromide |
| OPLS-DA | Orthogonal partial least squares discriminant analysis |
| PCA | Principal component analysis |
| PI | Propidium iodide |
| PVDF | Polyvinylidene difluoride |
| QTRAP | Triple quadrupole-linear ion trap mass spectrometer |
| ROS | Reactive oxygen species |
| SD | Standard deviation |
| TBST | Tris-buffered saline with 0.1% Tween 20 |
| TNF- α | Tumor necrosis factor- α |
| VEGF | Vascular endothelial growth factors |
| VIP | Variable importance in projection |

Colorectal cancer (CRC) is a prevalent form of cancer across the globe, ranking as the third most common type of cancer and the second highest contributor to cancer-related deaths. Its incidence and mortality are increasing in individuals under 50 years old^{1,2}. The incidence of CRC varies greatly from region to region in the world and is more elevated in developed nations when contrasted with developing nations. Generally, the frequency of CRC is typically one-third lower in women than in men³. The pathophysiological process of CRC involves various factors, with apoptosis playing a crucial mediating role. Apoptosis, as a regulated cell death mechanism, is often dysregulated in malignant cells^{4,5}, which mainly includes exogenous and intrinsic pathways, and mitochondria are considered to have a significant impact on intrinsic-apoptosis^{6,7}. Mitochondrial dysfunction can cause a decrease in MMP and the opening of the mitochondrial permeability transition pore (MPTP), which can directly stimulate the apoptotic pathway^{8,9}. Furthermore, mitochondria, as the primary producer of intrinsic ROS, are also vulnerable to ROS harm. Excessive ROS could result in oxidative DNA harm and trigger the mitochondria-mediated intrinsic apoptotic pathway, either caspase-dependent or independent¹⁰. Irregular cell cycle events contribute to the never-ending proliferation of cancer cells, in addition to apoptosis^{11,12}. PI3K/AKT/mTOR signaling pathway is an important signal transduction pathway in cells, which is involved in cell survival, proliferation, differentiation, apoptosis and other biological functions. It is mainly composed of phosphatidylinositol-3-kinase (PI3K), serine/threonine protein kinase AKT (also known as PKB), and mammalian target of rapamycin (mTOR)¹³. The PI3K/AKT/mTOR pathway regulates apoptosis by influencing mitochondrial function. The activation of AKT can control the apoptosis process by regulating the activity of pro-apoptotic proteins such as Bax and Bad in the Bcl-2 family proteins and the activity of caspase-9 and Caspase-3 in the caspase family proteins. Overexpression of Bcl-2 can inhibit AKT phosphorylation, thereby reducing mTOR activity, which may help to inhibit cell hyperproliferation and promote apoptosis¹⁴. In addition, Bcl-2 inhibits the activation of the caspase family by preventing the release of cytochrome c by mitochondria, which is a key step in initiating apoptosis¹⁵. In addition, AKT can also influence cell survival by regulating MMP and ROS levels. mTOR is mainly responsible for regulating cell growth and metabolism. It responds by sensing nutrients and growth signals, and promotes protein synthesis, glycolysis, mitochondrial function, and lipid synthesis, thereby affecting cell proliferation and survival. In addition, mTOR is also involved in the regulation of energy metabolism of immune cells, supporting the immune response¹⁶. In some cases, mTOR activity is associated with the development of cancer, such as in acute myeloid leukemia (AML), where the loss of mTORC1 can inhibit tumor progression¹⁷.

CRC is one of the most commonly diagnosed carcinomas worldwide. The use of chemotherapy and radiotherapy can lead to severe side effects and a decrease in the overall quality of life for patients¹⁸. Therefore, natural compounds are being explored as alternatives to conventional chemotherapeutic drugs due to their pharmacological safety and lack of side effects¹⁹. Alkaloids, nitrogenous organic compounds commonly found in natural products, have garnered increasing attention for their antitumor properties and specific mechanisms²⁰. Many different alkaloids that have been isolated from medicinal plants have demonstrated anti-proliferative and anticancer properties against a broad range of cancers, especially alkaloids from the genus *Zanthoxylum*²¹. Eth isolated from the *Z. bungeanum* in our lab is a common alkaloid component of the genus *Zanthoxylum*, especially in the species *Z. bungeanum* and *Z. armatum*. At present, there are relatively few pharmacological studies on Eth, and the existing researches mainly focus on the optimization of extraction process²² and the quality control of certain Chinese medicine as markers²³. Some studies have shown that there is an electrostatic force between Eth and human serum albumin (HSA), which can form a complex without fluorescence effect. In addition, chelerythrine (Eth homologue) has been proven to have anti-tumor²⁴, anti-inflammatory²⁵ and other pharmacological activities. Some related studies have shown that the plants *Z. bungeanum* and *Z. armatum*, which mainly contain Eth, have inhibitory effects on the proliferation of a variety of cancer cells, such as human laryngeal tumor cells, lung cancer cells, and human breast cancer cells^{26–28}. Studies

have also shown that *Zanthoxylum* plants can inhibit the proliferation of CRC cells and promote apoptosis²⁹, but the inhibitory effect of Eth on CRC proliferation has not been reported. In this study, we investigate the potential anti-colon cancer mechanism of Eth using a variety of molecular biological methods, as well as integrating proteomics and metabolomics.

Results

Eth inhibits colon cancer cell proliferation

The chemical structure of Eth was presented in Fig. 1A. As shown in Fig. 1B,C, Eth exhibited a dose-dependent reduction in the viability of HT29 and SW480 cells. Specifically, treatment with 24 μ M, 28 μ M, and 32 μ M Eth resulted in cell viabilities of 69.92%, 61.06%, and 49.08% for HT29 cells (Fig. 1B), and 55.20%, 49.52%, and 35.44% for SW480 cells (Fig. 1C), respectively. Given the more pronounced inhibitory effect on SW480 cells following Eth treatment, SW480 cells were chosen for the subsequent experiments under the 24 h treatment. Furthermore, the colony formation assay showed that chronic exposure to Eth led to a dose-dependent decrease in SW480 cell colonies (Fig. 1D,E). The above results indicated that Eth can effectively impede cell proliferation.

Eth induces apoptosis

Flow cytometry analysis revealed a dose-dependent increase in the level of apoptosis following treatment with Eth (24, 28, and 32 μ M), and the proportion of apoptosis increased from 0.11% (0 μ M) to 58.08% (32 μ M) (Fig. 2A,B). Moreover, western blot demonstrated an upregulation of p53 and Bax, and a downregulation of the apoptosis-related protein Bcl-2 (Fig. 2C) treated by Eth.

Eth causes cell cycle arrest in the G0/G1 phase

Flow cytometry analysis showed that Eth (24, 28 and 32 μ M) arrest cell cycle in the G0/G1 phase, with the cells proportion of G0/G1 phase increasing from 39.2% (0 μ M) to 75.42% (32 μ M), while G2/M phase decreasing from 38.00% (0 μ M) to 13.28% (32 μ M) (Fig. 3A,B). Additionally, Fig. 3C revealed that Eth down-regulated the expression of cyclin D1 protein and up-regulated the expression of p27 protein, both of which are related to the G0/G1 phase (Fig. 3C).

Effect of Eth on the mitochondrial-associated pathway in vitro

As shown in Fig. 4A–D, Eth treatment reduced the level of MMP in a dose-dependent manner in SW480 cells, whereas ROS level increased. Further, western blot analysis revealed an increase in the expression of cytochrome C (Cyt C) and Bax in the cytoplasm, a decrease in Bcl-2, and cleaved caspase-3 treated by Eth (Fig. 4E). Additionally, we also observed that the expression of poly (ADP-ribose) polymerase (PARP), an important downstream regulator of the mitochondria-associated pathways, increased following Eth treatment. In addition, 3-(4, 5-dimethylthiazol-2-yl)-2, 5-diphenyltetrazolium bromide (MTT) showed that proliferation inhibitory of Eth on SW480 was reversed by Z-VAD-FMK, an inhibitor that inhibits the effects of mitochondrial apoptosis³⁰.

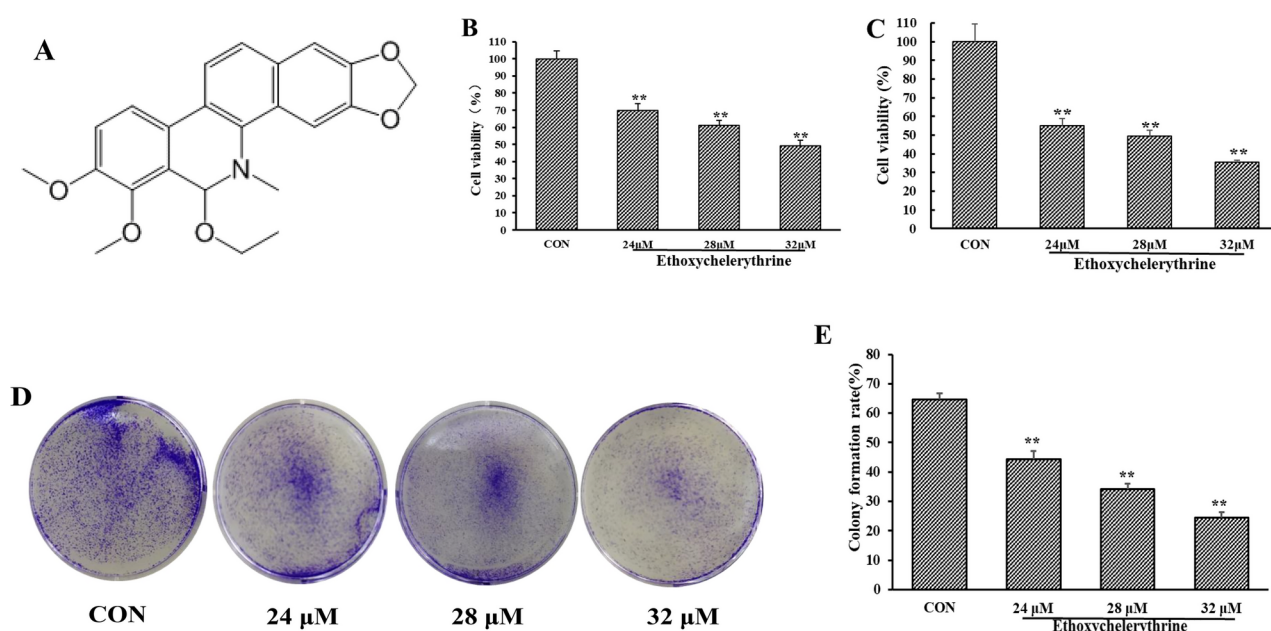


Fig. 1. Effect of different concentrations of Eth (24, 28 and 32 μ M) on the colon cancer cells proliferation. (A) Structure of Eth. (B,C) Effect of Eth on HT29 (B) and SW480 (C) cells viability for 24 h. (D,E) Effect of Eth on SW480 cell colony formation and colony formation rate. Data shown are means \pm SD (n = 6). * P < 0.05, ** P < 0.01 compared to the CON.

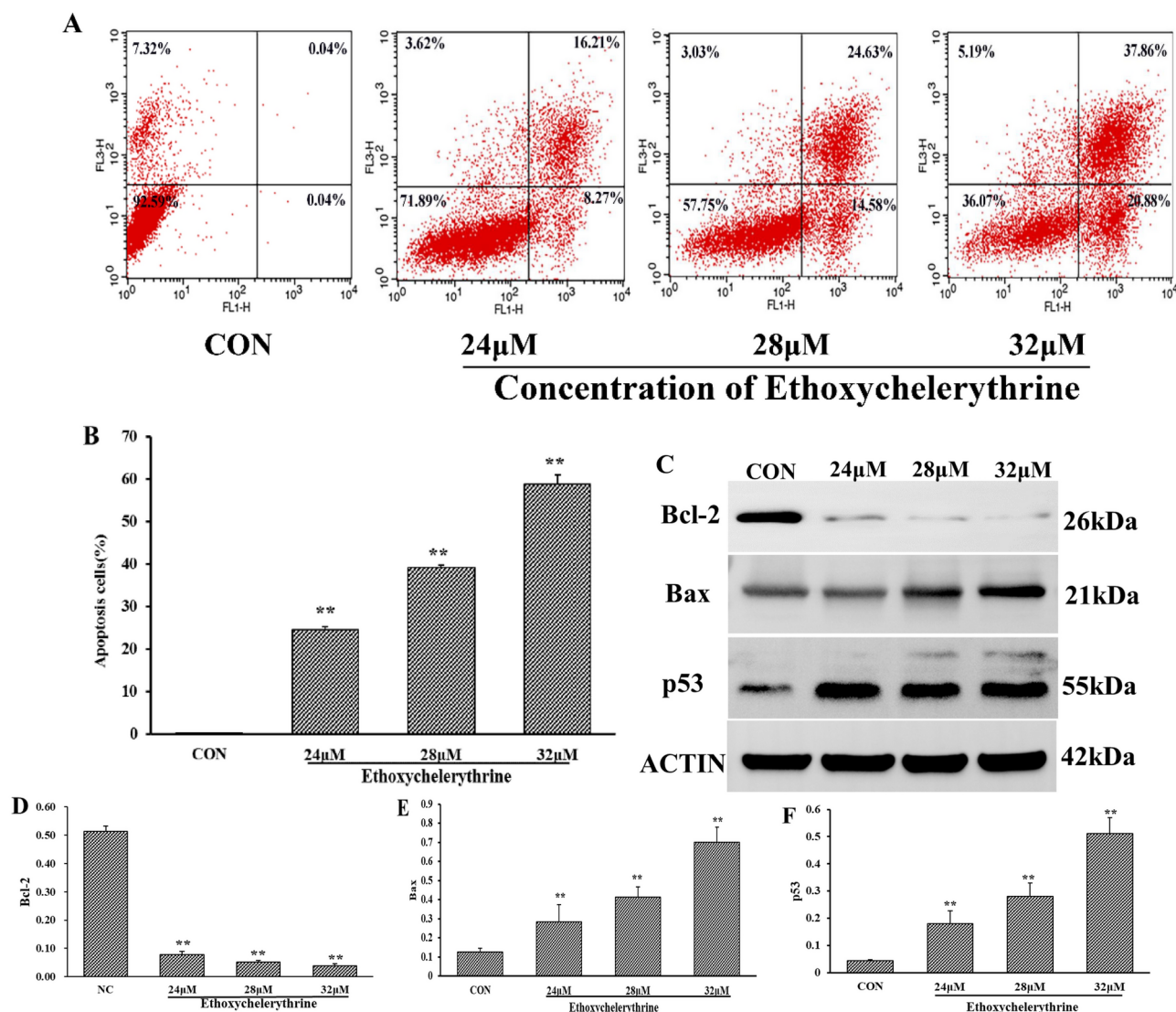


Fig. 2. Effect of Eth (24, 28 and 32 μ M) on the apoptosis level of SW480 cells. (**A,B**) Apoptosis level in Eth-treated SW480 cell. (**C**) The expressions of p53, Bcl-2, Bax in Eth-treated SW480 cell were measured by WB. The relative protein densities of (**D**) Bcl-2, (**E**) Bax, (**F**) p53. Data shown are means \pm SD ($n = 6$). * $P < 0.05$, ** $P < 0.01$ compared to the CON. Original blots of figure are presented in Supplementary Information.

The effect of Eth on the growth of SW480 xenograft tumor

Eth-treated mice received oral gavage administration for 21 days. The results showed the average tumor volume in the MOD group was 1630.71 mm³, and the tumor volume of Eth groups (L, M, and H) and positive control group (5-fluorouracil, 5-FU) were 1131.41 mm³, 905.72 mm³, 647.47 mm³ and 748.91 mm³, respectively. Compared with the MOD group, the Eth and 5-FU groups was significantly reduced the tumor volume (Fig. 5A,B). In addition, Eth treatment can also significantly reduce tumor weight, as evidenced by the average weight in the MOD group was 0.84 g, while in the L, M, H and 5-FU groups were 0.53 g, 0.28 g, 0.23 g and 0.28 g (Fig. 5C). The tumor inhibition rates were 36.90%, 66.67%, 72.61% and 66.64%, respectively. Meanwhile, the weight in the Eth treatment and 5-FU groups was increased compared with the MOD group (Fig. 5D). Subsequently, the spleen index analysis shown that a decrease in the MOD group, which was restored to levels similar to the CON group after Eth treatment, indicating a return to normal levels. (Fig. 5E).

Effect of Eth on the vascular endothelial growth factors (VEGF), basic fibroblast growth factor (bFGF), inter-leukin 6 (IL-6) and tumor necrosis factor- α (TNF- α) in serum of SW480 xenograft tumor nude mice

The secretions of VEGF and bFGF in serum were measured. The secretions of VEGF and bFGF were significantly decreased following treatment with Eth and 5-FU compared to the MOD group (Fig. 6A,B). As shown in Fig. 6C,D, the secretions of IL-6 and TNF- α were decreased by treatment with Eth and 5-FU.

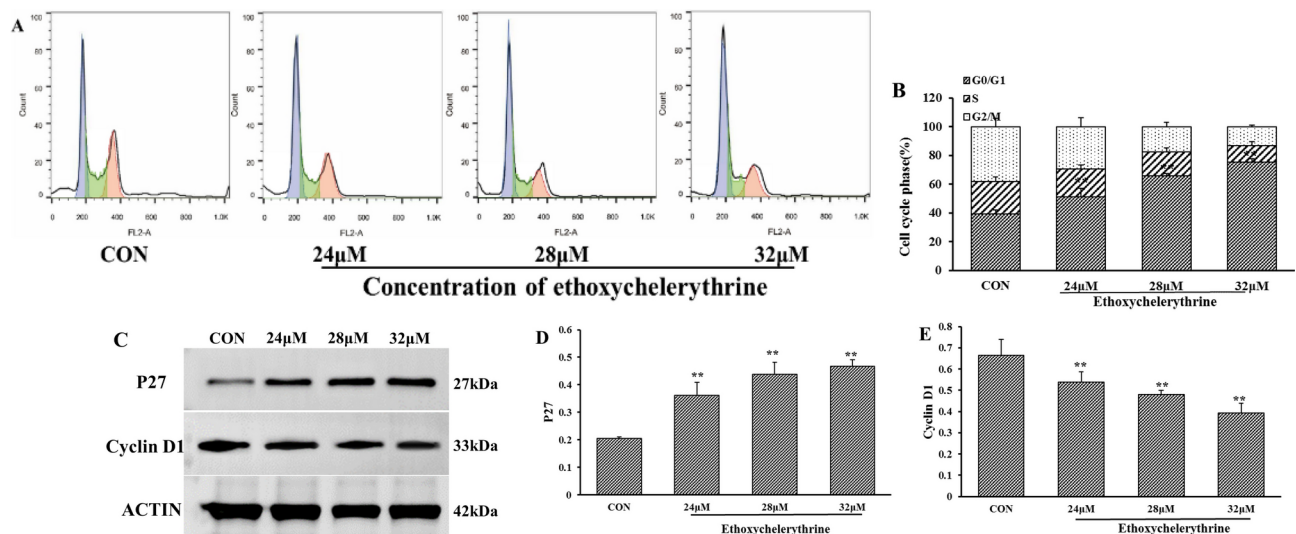


Fig. 3. Effect of Eth on the cell cycle of SW480 cells. (A,B) Flow cytometry analysis of cell cycle in Eth-treated SW480 cell. (C) The expression of P27, Cyclin D1 in Eth-treated SW480 cell were measured by WB. The relative protein densities of (D) P27, (E) Cyclin D1. Data shown are means \pm SD (n = 6). * P < 0.05, ** P < 0.01 compared to the CON. Original blots of figure are presented in Supplementary Information.

Effect of Eth on the Ki67, E-Cadherin, N-Cadherin of SW480 xenograft tumor

As depicted in Fig. 7A–C, Eth significantly reduced the expressions of Ki67 and N-cadherin while increased E-cadherin expression compared to the MOD group. This was further validated by immunohistochemistry, which demonstrated a down-regulation of Ki67 and N-cadherin expressions and an up-regulation of E-cadherin expression following Eth treatment (Fig. 7D–F). The above results were consistent with the qRT-PCR result.

Eth inhibits tumor proliferation through the mitochondrial apoptosis

We investigated the molecular mechanism of Eth treatment in vivo using SW480 xenograft tumors. Western Blot analysis of tumor tissue (Fig. 8A) showed that Eth promoted the expressions of Cyt C, Bax, p53, cleaved caspase3 and cleaved caspase9 (Fig. 8C–G) while reducing Bcl-2 protein level (Fig. 8B).

Serum proteome analysis

Proteomic revealing that 1486 proteins were analyzed and identified in the serum. Fold change of more than 1.5 was considered significantly upregulated whereas fold change of less than 0.6667 was considered significantly down-regulated in the two samples. 94 and 108 proteins were up-regulated and down-regulated in the MOD group, respectively. At the same time, 27 and 35 proteins were up-regulated and down-regulated in the Eth group (Fig. 10B,C). Furthermore, 23 of the differential proteins identified in the CON vs. MOD group were completely reversed by Eth treatment. Among them, 15 differential proteins, including LDHB, maltase glucoamylase (MGAM), HtrA serine peptidase 1 (HTRA1), GSS, Proprotein convertase subtilisin/kexin type 9 (PCSK9) and UDP-glucose pyrophosphorylase 2 (UGP2), are known CRC markers that can be involved in the colon cancer, and they interact with each other (Fig. 9D).

Most of the proteins are located in extracellular regions and cellular fractions and are involved in molecular functions, including protein binding, catalytic activity, etc. (Fig. 9E). KEGG showed that the complement and coagulation cascades between CON and MOD groups were enriched with the most proteins, from the KEGG enrichment analysis top20 bubble plots show that complement and coagulation cascades, Cholesterol metabolism, Protein digestion and absorption, and PI3K-Akt signaling pathway were enriched with more proteins (Fig. 9F). Meanwhile, KEGG results showed that the complement and coagulation cascades, Cysteine and methionine metabolism, Cholesterol metabolism, PI3K/Akt signaling pathway between MOD and Eth groups were enriched with the most proteins (Fig. 9G). In further literature review, the PI3K/AKT signaling pathway captured our attention, as it is highly associated with tumorigenesis according to published reports. After Eth intervention, Lamb1 and Col1a1 proteins were enriched in the PI3K/AKT pathway and they could also interact with 14 colon cancer tumor markers, see Fig. 9

Eth exerts anticancer by inhibiting PI3K/Akt/mTOR pathway in SW480 xenograft tumors

As shown in Fig. 10A–D, high expression of p-PI3K, p-AKT and p-mTOR were significantly inhibited after Eth intervention, suggesting that Eth may act by targeting the PI3K/AKT/mTOR signaling pathway.

Serum metabolomics analysis

Metabolomics analysis showed that the 965 metabolites identified in serum could be grouped into 12 known classes (Table S2). The supervised OPLS-DA parameters for the classification shown excellent performance on predictive ability (Fig. 11A,B). The metabolic profile of the Eth group was similar to that of the CON group,

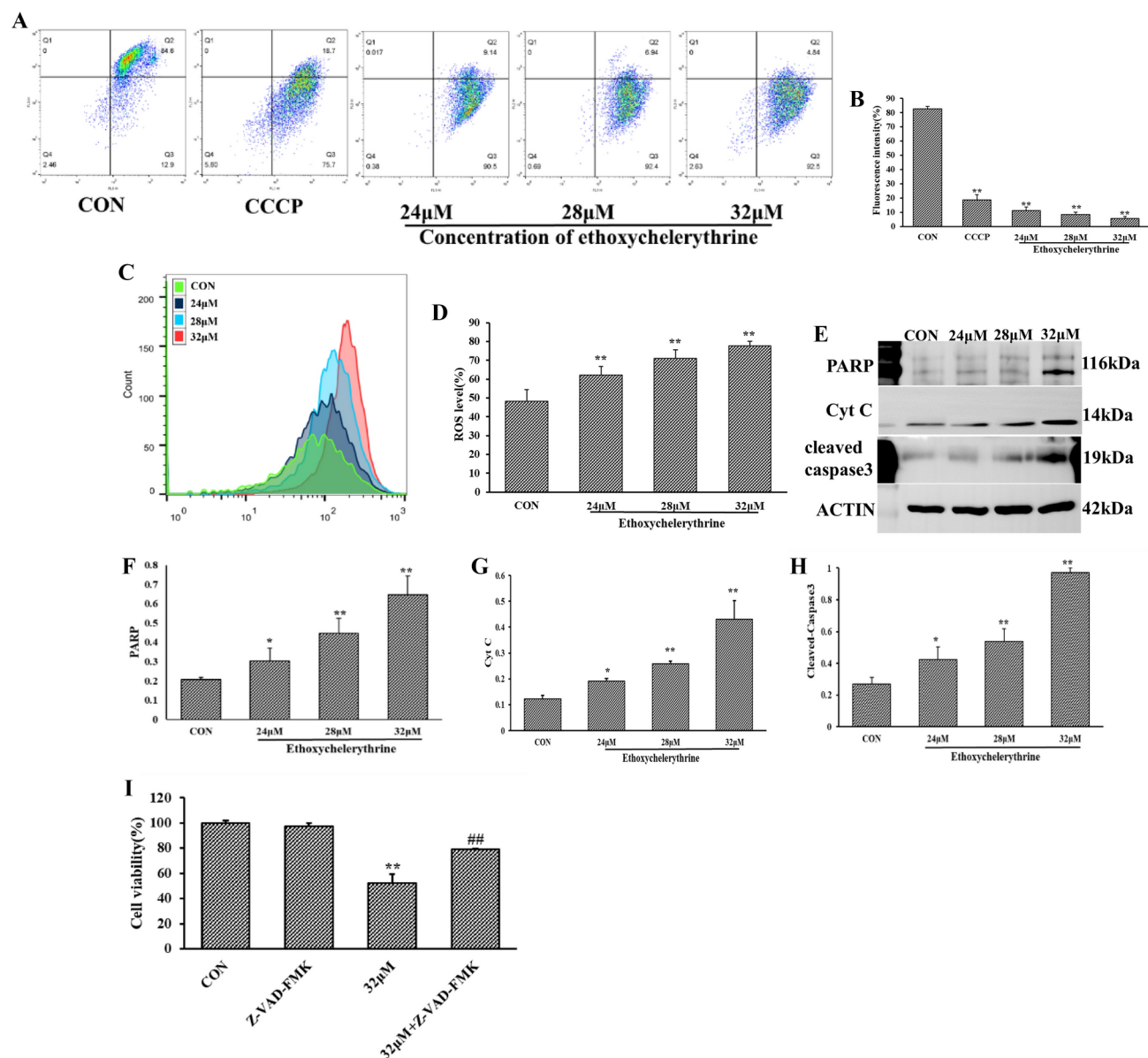


Fig. 4. Effect of Eth on the mitochondrial apoptosis of SW480 cells. (A–D) Flow cytometry analysis of MMP (A) and ROS (C) in Eth-treated SW480 cells and the quantification results (B,D), respectively. (E) Western blot analysis of PARP, Cyt C, and Cleaved caspase3 in Eth-treated SW480 cells. The relative protein densities of (F) PARP, (G) Cyt C, (H) Cleaved caspase3. (I) Effect of 32 μM Eth on the cell viability in the presence or absence of 10 μM Z-VAD-FMK was determined by MTT. Data shown are means ± SD (n = 6). *P < 0.05, **P < 0.01 compared to the CON. ##P < 0.01 compared to the 32 μM + 10 μM Z-VAD-FMK. Original blots of figure are presented in Supplementary Information.

both showing significant separation from the MOD group. Metabolites that were significantly different in the CON vs. MOD group and Eth vs. MOD group are shown as volcano plots (Fig. 11C,D). Further, 191 metabolites (up-regulated 92, such as L-homocitrulline, 3-indolepropionic acid, carnitine C13:1, carbamoyl phosphate; down-regulated, 99, such as cytosine, cytidine, cyromazine, 2-O-methylcytosine) in CON vs. MOD, and 106 metabolites (up-regulated 47, such as geranic-acid, cyromazine, galactitol, N-acetyl-L-glutamic Acid; down-regulated, 59, such as carbamoyl phosphate, carnitine C11:1, carnitine C13:1, succinic anhydride) in Eth vs. MOD were identified (Fig. 11D, Table S3). As shown in Fig. 11E,F, many different metabolites are enriched in the pyrimidine metabolism, and the most metabolites in this pathway are significantly regulated after Eth intervention.

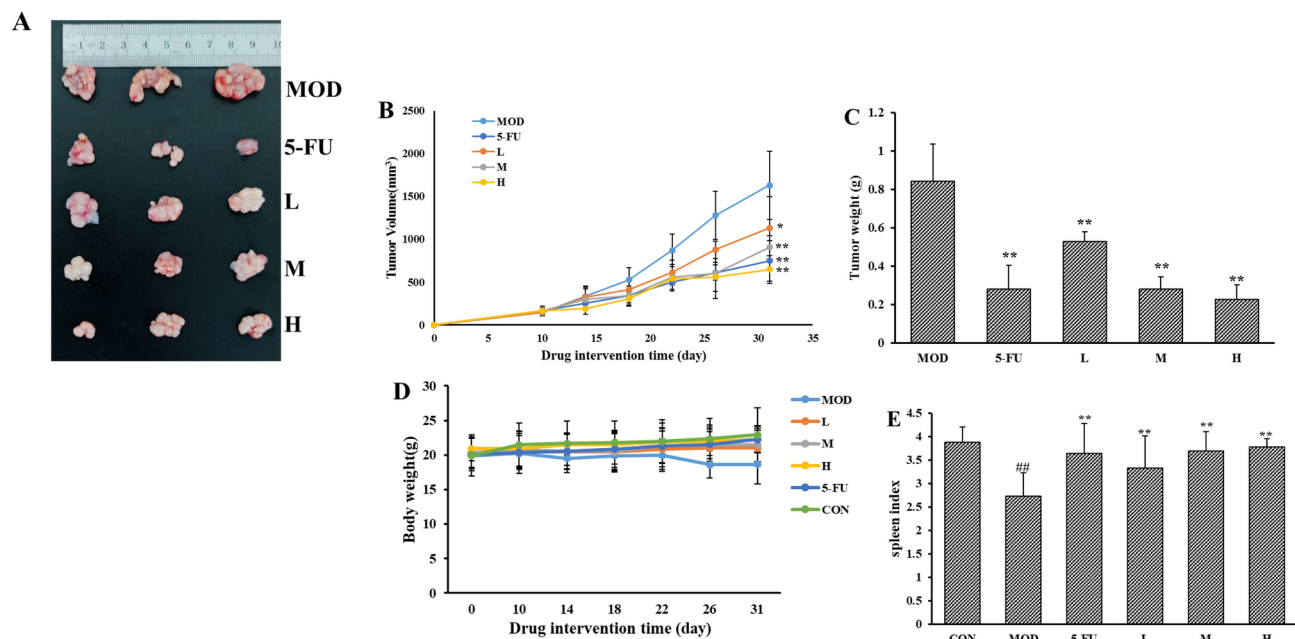


Fig. 5. Effect of Eth on the proliferation of SW480 xenograft tumor. **(A)** Tumor specimens obtained after day 29 of inoculation. **(B,C)** Effect of Eth on the volume and weight of SW480 xenograft tumor. **(D,E)** Effect of Eth on the body weight and spleen index of SW480 xenograft tumor nude mice. Data shown are means \pm SD ($n=10$). * $P<0.05$, ** $P<0.01$ when compared to the MOD, ## $P<0.01$ compared to the CON group.

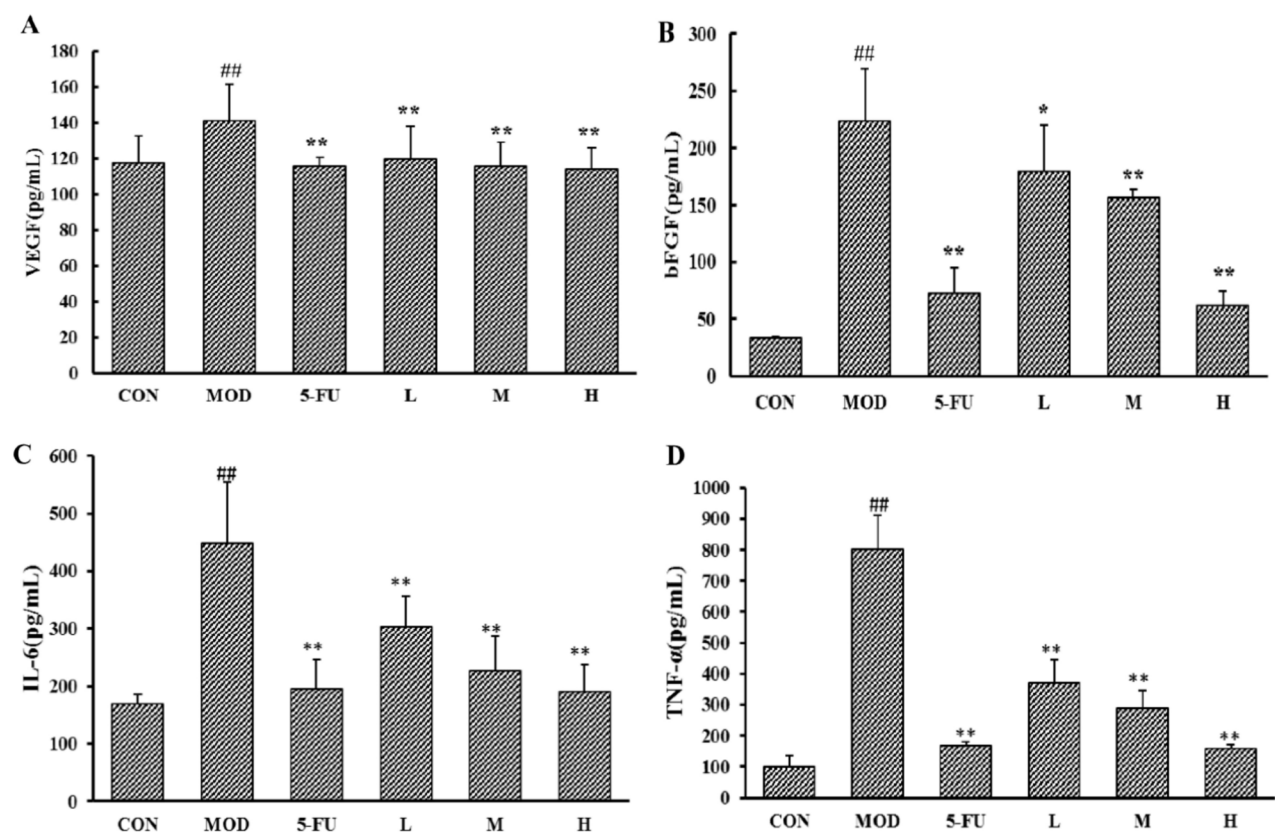


Fig. 6. The effect of Eth on the cytokine in serum of SW480 xenograft tumor nude mice. **(A–D)** ELISA analysis of the expressions of VEGF **(A)**, bFGF **(B)**, IL-6 **(C)** and TNF- α **(D)** in the serum of nude mice. Data shown are means \pm SD ($n=10$). ** $P<0.01$ compared to the MOD group, * $P<0.05$, ## $P<0.01$ compared to the CON group.

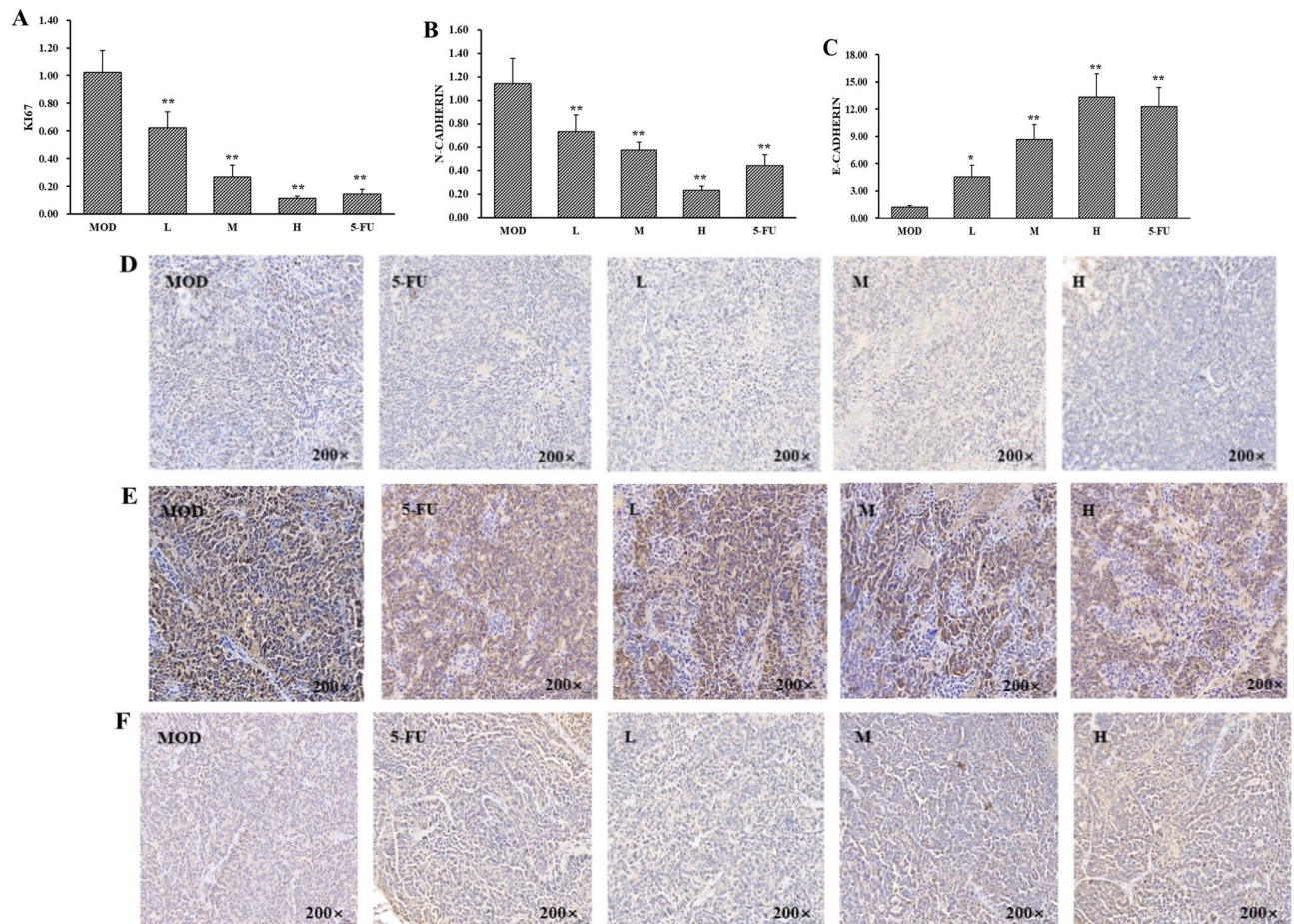


Fig. 7. Effect of Eth on the Ki67, E-Cadherin and N-Cadherin of SW480 xenograft tumor. qRT-PCR analysis of (A) Ki67, (B) N-Cadherin, (C) E-Cadherin in Eth-treated SW480 xenograft tumor mice. Immunohistochemistry analysis of (D) Ki67, (E) N-Cadherin, (F) E-Cadherin in Eth-treated SW480 xenograft tumor mice. Data shown are means \pm SD (n = 10). * P < 0.05, ** P < 0.01 compared to the MOD group.

Comprehensive analysis of differential metabolites and differential proteins in serum of SW480 xenograft tumor mice

Further, we constructed a protein-metabolite correlation network ($|r| \geq 0.8$ and $P < 0.05$) (Table S4). The hierarchical heatmap (Fig. 12A) showed that differential metabolites involved in pyrimidine metabolism were closely correlated with differential proteins. 9 proteins and 22 metabolites within nodes included 9 correlations and 26 negative correlations (Fig. 12B). Among them, differential protein Gss was negatively correlated with differential metabolites Cytidine, Cytosine, Deoxycytidine, Epoxy-eicosapentaenoic-acid, and Hydroxyeicosapentaenoic-acid, and LDHB was negatively correlated with differential metabolites Cytidine, Cytosine, Deoxycytidine. These metabolites are mainly enriched in the Pyrimidine pathways.

Discussion

Our study demonstrates the anti-colorectal cancer effects of Eth on SW480 and HT29 cells, with a more pronounced inhibitory effect on SW480 cells. In this study, we used multi-omics and multi-methods to demonstrate that Eth can target and inhibit the PI3K/AKT/mTOR signaling pathway to exert anti-colorectal cancer effects.

Apoptosis plays a crucial role in cancer pathogenesis, following two basic mechanisms, intrinsic (mitochondrial-mediated cell death) and extrinsic (death receptor-mediated)³¹. Studies have established the crucial implication of mitochondria in the process of apoptosis. Some early events including alterations in MMP, generation of ROS and release of Cyt C are always accompanied by apoptosis mediated by the mitochondrial pathway^{32,33}. In addition, mitochondrial apoptosis is regulated by a variety of apoptosis regulators³⁴. The reduced expression of Bcl-2 protein and elevated expression of Bax protein induce permeabilization of the outer mitochondrial membrane and accumulation of ROS, which leads to the release of Cyt C, causing the cascade reaction of caspase and split of PARP^{35–37}. Caspase-3, a crucial apoptotic protein in the caspase cascade reaction, can be activated by the complex formation of Cyt C and caspase-9³⁸. PARP, as a target protein of caspase-3, is also involved in the process of apoptosis^{39,40}. Our study determined that Eth markedly inhibited the proliferation of SW480 cells and arrested at the G0/G1 phase. Meanwhile, flow cytometry results showed that Eth could

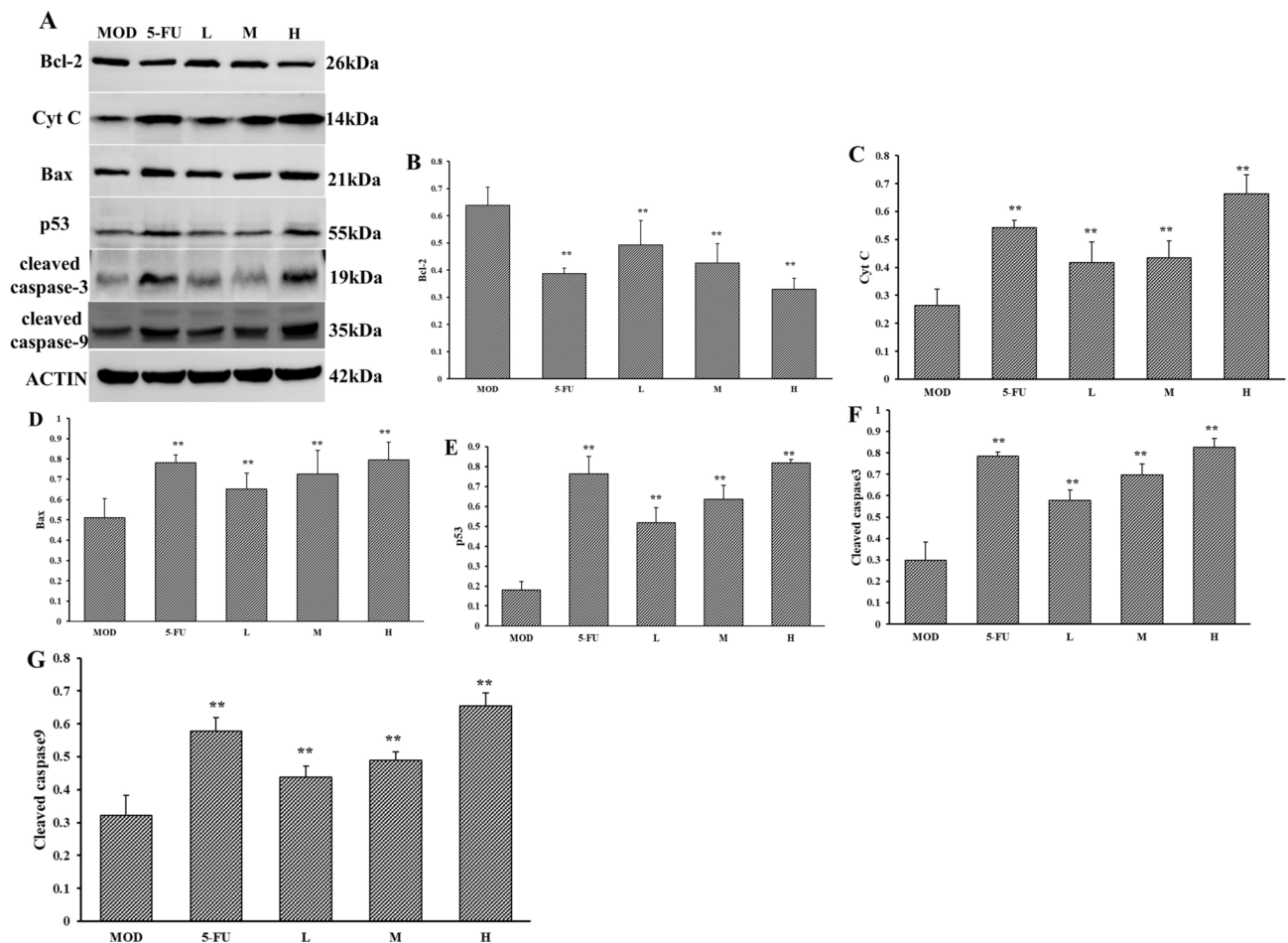


Fig. 8. Effect of Eth on the apoptosis-related proteins of SW480 xenograft tumor mice. (A) Bcl-2, Cyt C, Bax, p53, cleaved caspase3 and cleaved caspase9 in Eth-treated SW480 xenograft tumor mice were analysis by Western blot. The relative protein densities of (B) Bcl-2, (C) Cyt C, (D) Bax, (E) p53, (F) Cleaved caspase-3, (G) Cleaved caspase-9. Data shown are means \pm SD (n = 10). * P < 0.05, ** P < 0.01 compared to the MOD group. Original blots of figure are presented in Supplementary Information.

induce apoptosis, decrease MMP level and increase ROS level in SW480 cells. Moreover, Eth downregulated the expression of Bcl-2 and upregulated the Bax, and Cyt C, thereby accelerating the activation of pro-apoptotic proteins caspase-3 and elevating PARP expression. Further experiments revealed that the proliferation inhibitory of Eth was reversed by the Z-VAD-FMK, a apoptosis inhibitor.

In addition to its role in cellular processes such as apoptosis, cell cycle arrest, and cell senescence, the tumor suppressor p53 is a crucial guardian of cellular genomes⁴¹. Research have demonstrated that p53 can not only trigger the release of pro-apoptotic factors to promote apoptosis but also control cell growth arrest^{42,43}. In this research, Eth treatment upregulated the expressions of p53 and P27 and downregulated the expression of Cyclin D1, leading to cell cycle arrest at G0/G1 phase. Subsequent antitumor experiments in vivo revealed that Eth significantly decreased the volume and weight of xenografts tumor, while western blot results showed that Eth upregulated the expressions of Bax, cleaved caspase3, cleaved caspase9, Cyt C and p53, and downregulated the expression of Bcl-2.

As we know, in the process of tumor development and metastasis, pro-angiogenic factors such as VEGF and bFGF exert play a crucial role in enabling tumor cells to enter the bloodstream and form distant metastases^{44,45}. VEGF is known to be a key player in the proliferation and angiogenesis of induced endothelial cells⁴⁶. Additionally, bFGF has been found to enhance the expression of VEGF in endothelial cells, acting synergistically with VEGF⁴⁷. The induction of angiogenesis by VEGF/bFGF is identified as a critical step in tumor proliferation and migration⁴⁸. Epithelial-mesenchymal transition (EMT) was a vital tumor event that promoted cancer cell metastasis⁴⁹. Epithelial cells acquire migratory and invasive properties through the EMT process. This transformation is characterized by the loss of epithelial markers (e.g., E-cadherin) and the gain of mesenchymal markers (e.g., N-cadherin)⁵⁰. Pharmacologic interventions to fight inflammation in cancer may slow cancer progression. In this research, we found that Eth could reduce the secretions of serum VEGF, bFGF, IL-6 and TNF- α in mice, down-regulate the expression of Ki67 and N-cadherin, up-regulate E-cadherin, which indicates that Eth can inhibit angiogenesis and inflammation, and inhibit the EMT process of SW480 cells.

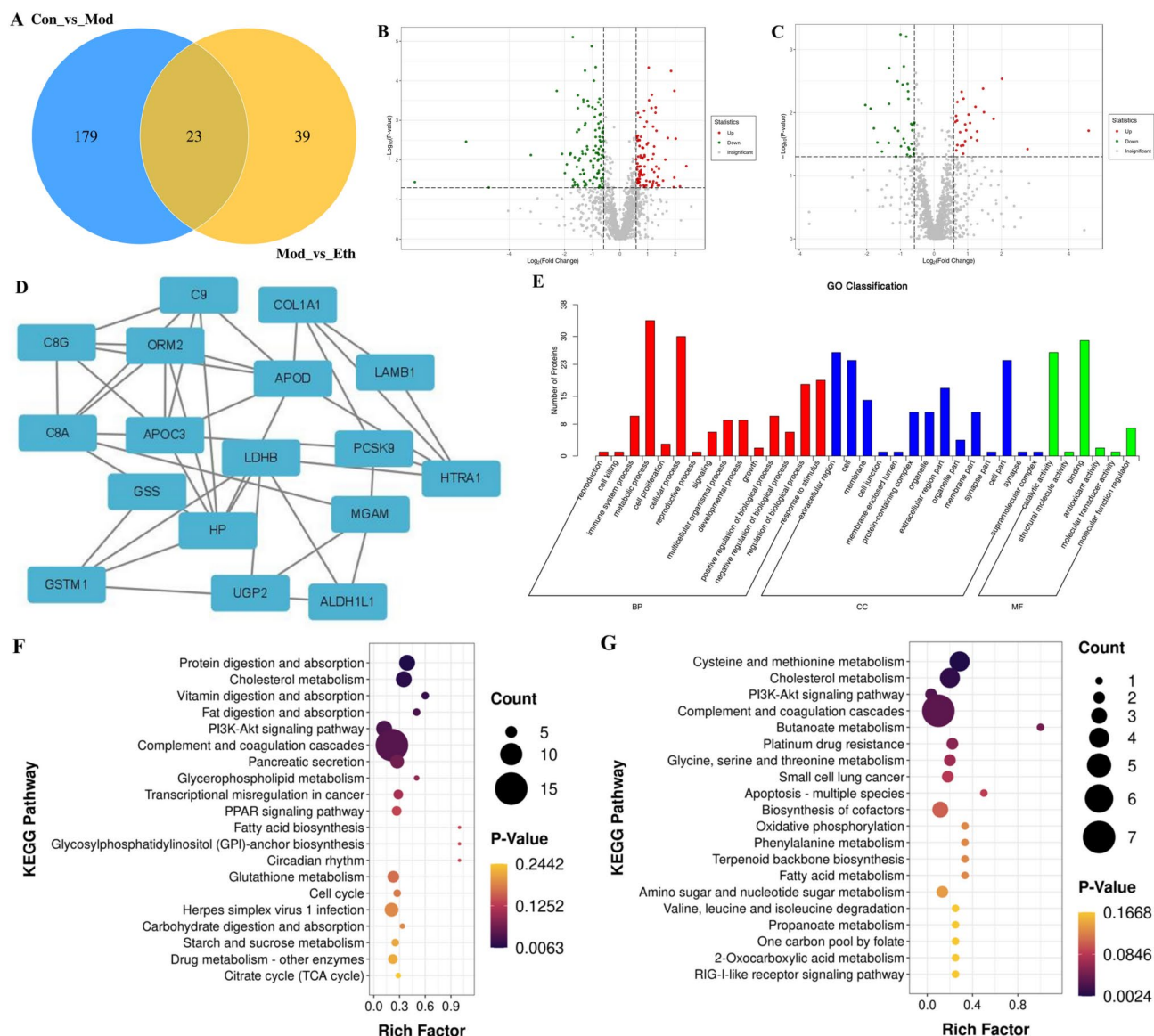


Fig. 9. Effect of Eth on the serum proteomics in SW480 xenograft tumor mice. **(A)** Differential proteins between CON and MOD groups and between MOD and Eth groups were shown by Venn diagram depicting. The up- and down-regulated proteins between CON and MOD groups **(B)** and between MOD and Eth groups **(C)** were depicted by Volcano plots. **(D)** PPI plots of key differential proteins between MOD and Eth groups. **(E)** GO functional enrichment analysis of differentially expressed proteins between MOD and Eth. Bubble plots depicting the KEGG enrichment analysis of differential proteins between CON and MOD **(F)** and between MOD and Eth **(G)**. The color and size of the dots means the p-value and the number of enriched differential proteins.

Proteomics results showed 23 of the differential proteins in the CON vs. MOD group were completely reversed after Eth treatment. LDHB is an acetylated protein that promotes the tricarboxylic acid (TCA) cycle and was also highly expressed in CRC cells^{51,52}. Our data also show that Eth reverses the high expression of LDHB in CRC mice. MGAM is an intestine-specific protein required to catalyze starch catabolism, and its expression is reduced in human CRC cells compared to normal intestinal epithelial cells⁵³. There is evidence that HTRA1, which is downregulated or even lost in a variety of primary and metastatic tumors, acts as a tumor suppressor⁵⁴ and the upregulation of HTRA1 contributes to the inhibition of cancer cell proliferation and tumor growth in vitro⁵⁵. Notably, our results also show that the expression of MGAM and HTRA1 is downregulated in CRC mice and they are elevated in mouse serum by Eth intervention. GSS, which encodes glutathione synthetase, regulates glutathione synthesis, an important component of the ROS scavenging system, and studies have found that the loss of intracellular glutathione makes cancer cells more susceptible to chemotherapeutic agents⁵⁶. PCSK9 is a secreted serine endoprotease that can be biosynthesized by several species and is essential in regulating lipid metabolism. In animal studies, deletion of the PCSK9 gene or inhibition of the PCSK9 protein inhibited

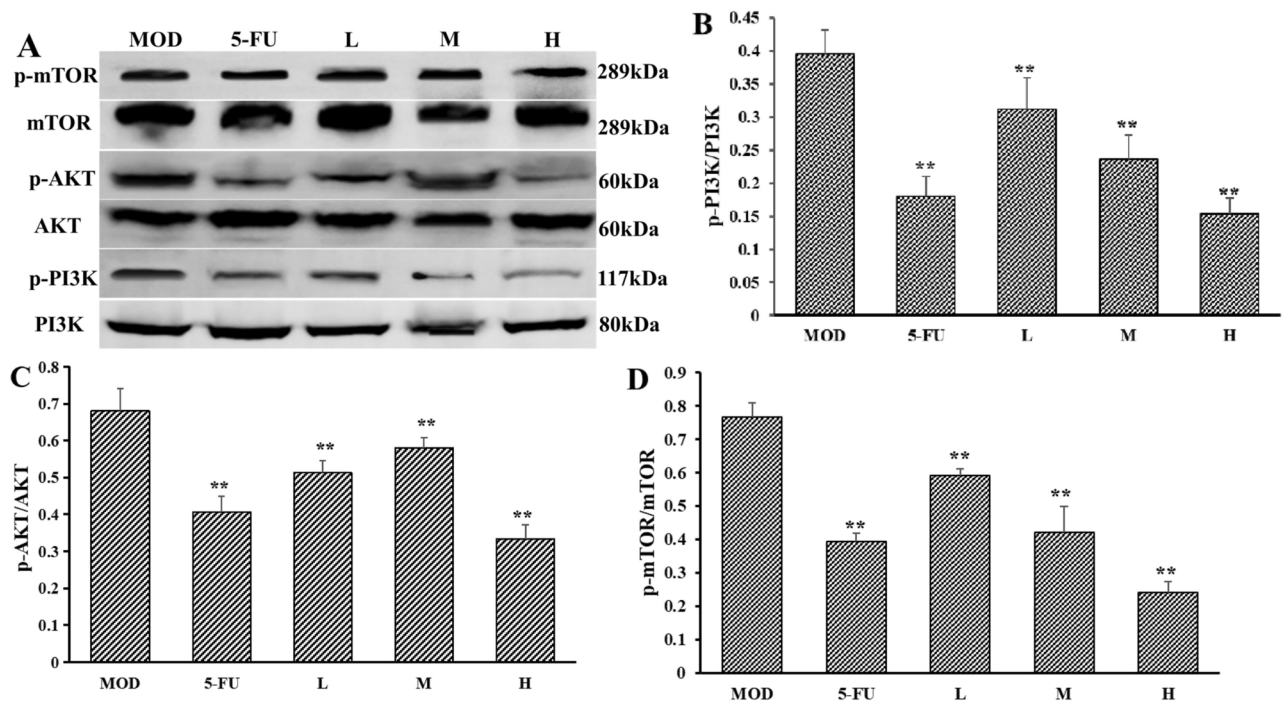


Fig. 10. Effect of Eth on the proteins in the PI3K/Akt/mTOR pathway of SW480 xenograft tumor mice. (A) Western blot analysis of PI3K, p-PI3K, AKT, p-AKT, mTOR and p-mTOR in Eth-treated SW480 xenograft tumor mice. The relative protein densities of (B) p-PI3K, (C) p-AKT, (D) p-mTOR. Data shown are means \pm SD (n = 10). **P < 0.01 compared to the MOD group. Original blots of figure are presented in Supplementary Information.

tumor growth⁵⁷. Our results showed that the expression of Gss and Pcsk9 decreased to a normal level by Eth intervention.

Meanwhile, KEGG showed that many differential proteins in CON vs. MOD and MOD vs. Eth group are enriched into PI3K/Akt signaling pathway, which was highly associated with tumorigenesis and captured our attention. LAMB1 and COL1A1 as significantly modulated by Eth can interact with other 15 differential proteins as tumor markers mentioned above. It was reported LAMB1 activates PI3K signaling molecules, and then PI3K activates its downstream molecule Akt and further induces collagen COL1A1 expression^{58,59}. PI3K/Akt/mTOR pathway is a major cancer-related signaling cascade⁶⁰. We revealed that Eth inhibits the activation of PI3K/Akt/mTOR pathway by suppressing the expression of related proteins (p-PI3K, p-Akt, and p-mTOR).

We further explored the global metabolic profile of xenografted nude mice with Eth administration by metabolomics. After the Eth intervention, 47 differential metabolites in the serum tended to normal level. Among these, many metabolites involved in the development of CRC can be regulated by PI3K/Akt/mTOR signaling pathway. The Phe-Pro amino acid elevated by Eth could inhibit the growth of HT-29 cancer cells and induce apoptosis via the caspase-3 cascade⁶¹. The carbamoyl phosphate synthase 1 (CPS1), as one of the main enzymes catalyzing the generation of carbamoyl phosphate (CP), can synthesize CP using free ammonia as an amino donor⁶². CPS1 overexpression was positively associated with post-treatment tumor status and grade as well as patient survival⁶³. Notably, in our results, Eth intervention in xenografted nude mice significantly reduced serum CP levels. In addition, it has been reported that deoxycytidine kinase (dCK) can inhibit the CRC cells growth through activating cytosine arabinoside (ara-C)⁶⁴. Fan et al found that dCK can regulate cell migration and invasion through the AKT pathway⁶⁵. Peng et al found that 3, 6-dihydroxyflavone (3, 6-DHF), as an effective methyltransferase (DNMT)1 inhibitor, could inhibit the PI3K/Akt/mTOR pathway by to the putative cytosine pocket of this protein⁶⁶. Interestingly, Cao et al found that pogostone relies on inhibition of the PI3K/Akt/mTOR signaling pathway for its anticancer activity and induces apoptosis and autophagy in vitro and in vivo⁶⁷. Our results also found that Eth could increase the level of deoxycytidine, cytosine, and pogostone in the serum of xenografted mice. It is well known that cancer cells, as cells with abnormally vigorous metabolism, can produce numerous metabolites. A large body of evidence indicates the interaction of oncogenic signaling and pyrimidine synthesis in tumorigenesis, and pyrimidine metabolism dysfunction is closely related to cancer progression, and many drugs targeting pyrimidine metabolism have been approved for a variety of cancers, such as 5-FU^{68,69}. Notably, it has been shown that PI3K/Akt/mTOR promotes cancer progression by regulating pyrimidine metabolism⁷⁰. In our study, the pyrimidine metabolism was significantly affected by Eth.

Two-omics correlation analysis demonstrated significant correlation between differential metabolites and differential proteins, including 9 positive and 26 negative correlations. Differential protein Gss was negatively correlated with Cytidine, Cytosine, Deoxycytidine, Epoxy-eicosapentaenoic acid and Hydroxyeicosapentaenoic acid. It was reported that LDHB is a downstream target of mTOR and that activation of mTOR by AKT further

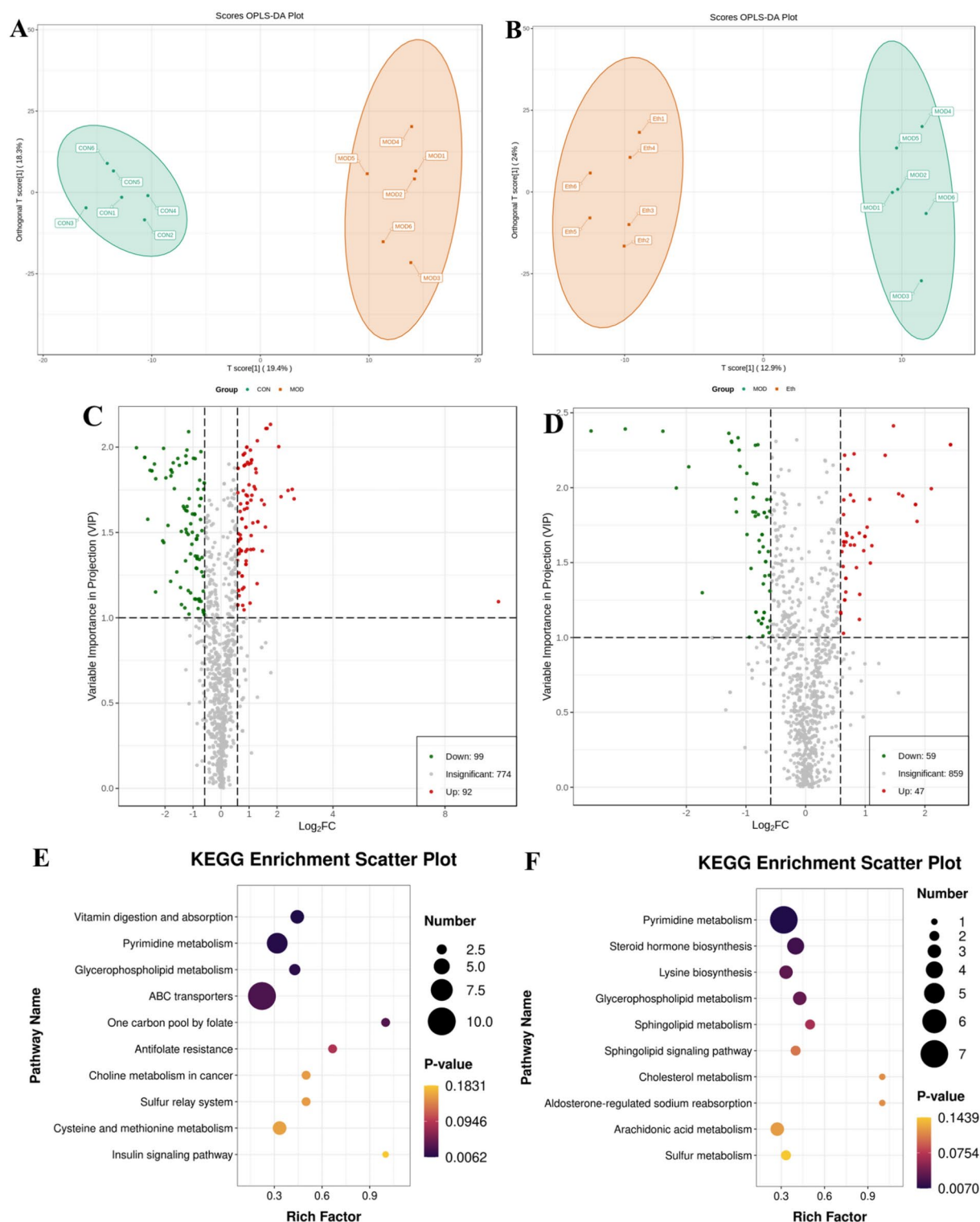


Fig. 11. Effect of Eth on the serum metabolomics in SW480 xenograft tumor mice. Score scatter plot of OPLS-DA for CON vs. MOD (A) and MOD vs. Eth (B). The up- and down-regulated metabolites between CON and MOD groups (C) and between MOD and Eth groups (D) were depicted by Volcano plots. (E,F) KEGG enrichment analysis of differential metabolites in serum of SW480 xenograft tumor mice. (E) CON vs. MOD, (F) MOD vs. Eth.

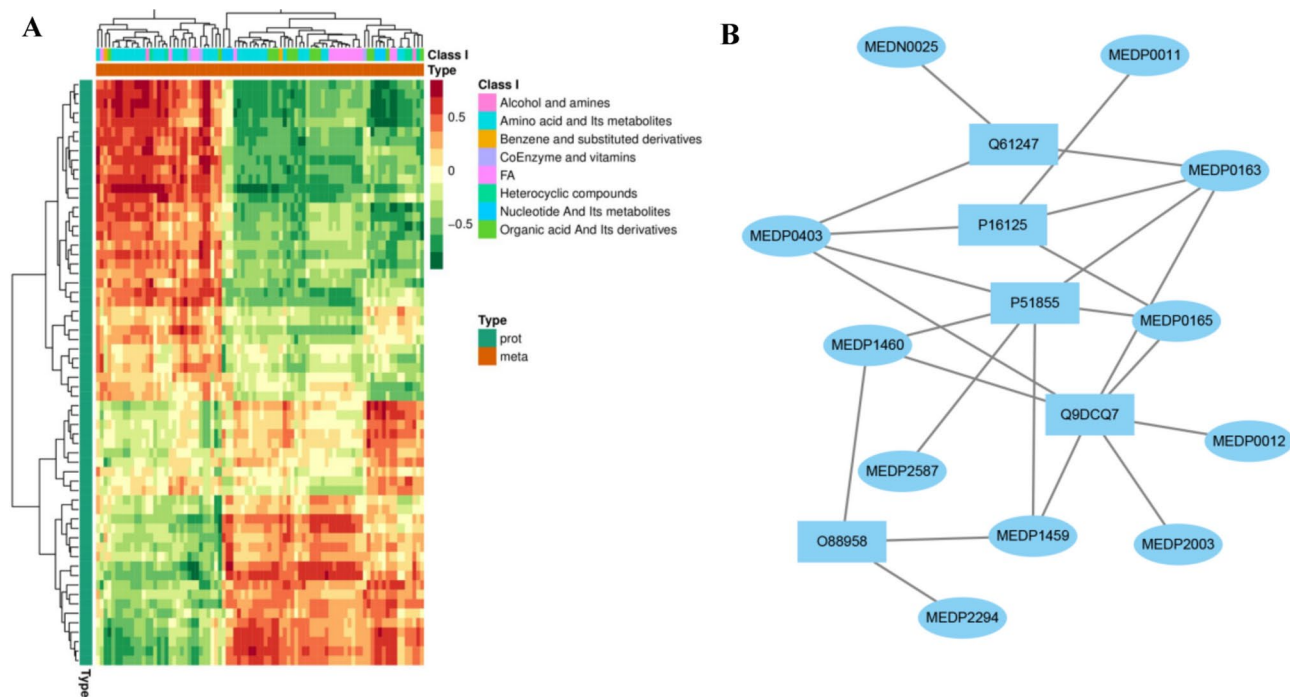


Fig. 12. Hierarchical clustering heatmap of differential proteins and metabolites. Matrix heat map showing correlation coefficient matrix for differential proteins and metabolites (A). Interaction network diagram of relevant proteins and metabolites after ETh intervention (B). Squares represent proteins and ovals represent metabolites.

upregulates LDHB expression during carcinogenesis⁷¹. LDHB has negatively correlated with differential metabolites Cytidine, Cytosine and Deoxycytidine, which were mainly enriched in the pyrimidine pathway.

Conclusions

In conclusion, Eth may exert its anti-tumor effect by inhibiting PI3K/AKT/mTOR pathway, activating mitochondrial apoptosis pathway, regulating a variety of metabolites and metabolic pathways, especially pyrimidine metabolism, and regulating multiple proteins such as Gss and LDHB. Eth may serve a therapeutic role for colon cancer patients in the future.

Materials and methods

Reagents and antibodies

Ethoxychelerythrine, partly of which was isolated from *Zanthoxylum armatum* by our laboratory with a purity $\geq 98\%$, and the remaining portion (Pufei De Biotech Co., Ltd, Chengdu, China); 5-Fu (Xudong Haipu Pharmaceutical Co., Ltd, Shanghai, China); primary antibodies β -actin (GB12001), p53 (GB111740), Bax (GB12690), Cytochrome C (Cyt C, GB12080), PARP (GB111501), CyclinD1 (GB111935), E-Cadherin (GB11082), N-Cadherin (GB11135) were purchased from Wuhan Servicebio Co., Ltd. cleaved-Caspase3 (ab2302), Bcl-2 (ab32124), and p27 (ab32034) were purchased from Abcam Technology (Cambridge, UK).

Cell culture

Human colon cancer cell lines, SW480 and HT29, were purchased from the National Biomedical Experimental Cell Resource Bank. Authentication of the SW480 and HT29 cells was conducted using short tandem repeat (STR) profiling within in the last 3 years. Cells were cultured using RPMI 1640 medium (SW480 cells, Solarbio, China) and DMEM (HT29 cells, Gibco, 11965084), both supplemented with 10% fetal bovine serum (Gibco, US), penicillin (100 U/mL) and streptomycin (100 μ g/mL) in a humidified atmosphere with 5% CO₂ at 37 °C. All experiments were performed with mycoplasma-free cells (National Biomedical Experimental Cell Resource Bank, Shanghai, China)

Cell viability assay

The cytotoxicity of Eth on SW480 and HT29 cells were evaluated using the MTT assay. Cells were seeded in 96-well plates at a density of 1×10^4 cells/well for 24 h and then exposed to Eth (24, 28 and 32 μ M) for 24 h, control cells (CON) were treated with a drug-free medium. After that, MTT (5 mg/mL, 20 μ L) was added and incubated for another 4 h. Finally, the 96-well plate was measured at 492 nm after adding 150 μ L dimethyl sulfoxide (DMSO).

Colony formation assay

Cells at a density of 1×10^3 cells/well in 6-well plates was exposed to Eth. After 24 h, the medium was switched to complete medium (containing 10% fetal bovine serum, 100 U/mL penicillin and 100 µg/mL streptomycin in RPMI 1640 medium) and incubated for another 14 days, during which time the medium was changed every 2 days. Following this, paraformaldehyde-fixed cells were stained with 0.1% crystal violet. Subsequently, the cells were gently washed and photographed for quantification.

Cell apoptosis

Cells were incubated in 6-well plates at a density of 1×10^5 cells/well for 24 h. Afterward, they were exposed to Eth (24, 28 and 32 µM) for another 24 h. Subsequently, the cells were stained with Annexin V-FITC and propidium iodide (PI) (Beijing Solaibio Technology Co., Ltd., China) after rinsed with pre-cooled PBS. The apoptosis level was measured and analyzed using Flow Jo V10 software.

Cell cycle assay

After being washed with pre-cooled PBS, Cells (1×10^5 cells/well) were fixed with 75% ethanol overnight after 24 h of treatment. The cell cycle was analyzed by measuring cellular DNA content using PI staining (Beijing Solaibio Technology Co., Ltd., China). Cell cycle ratios were measured and quantified by flow cytometry and Flow Jo V10 software.

ROS and MMP assay

Cells were exposed to Eth for 24 h and stained with fluorescent probe DCFH-DA (Beijing Solaibio Technology Co., Ltd., China) in darkness at 37 °C for 20 min to detect intracellular ROS. Similarly, another fluorescent probe JC-1 (Solaibio Technology Co., Ltd., Beijing, China) in darkness at 37 °C for 20 min was used to detect the level of MMP. Intracellular ROS and MMP levels were observed and quantified by flow cytometry and Flow Jo V10 software.

Human colorectal cancer xenografts in nude mice

All experimental protocols were approved by the Animal Ethics Committee of the Henan University of Chinese Medicine (DWLL202003253). All methods were carried out in accordance with relevant guidelines and regulations, and handled according to standard use protocols and animal welfare regulations, and we also confirmed that the animal study was reported in accordance with ARRIVE guidelines (<http://arriveguideline.org>). BALB/C nude mice (4–5 weeks, 20 ± 2 g) were purchased from Beijing Vital River Laboratory Animal Technology Co., Ltd. (SCXK 2012–0006, Beijing, China). SW480 cells were suspended in PBS at a density of 2×10^7 /mL and injected subcutaneously into the right forelimb of the mice in 200 µL. Additionally, another 10 BALB/C nude mice were injected subcutaneously with only 200 µL PBS, serving as the CON group. Upon reaching tumor volumes of approximately 100 mm³, the xenograft tumor mice were randomly divided into 5 groups (n = 10 per group): MOD group (orally treated with the vehicle 0.5% CMC-Na), Eth groups with low, middle, and high doses (4.5, 9 and 18 mg/kg of Eth solubilised using CMC-Na) and 5-FU group (25 mg/kg, intraperitoneal injection every 2 days). Mice in the CON and Eth groups were orally administered either Eth or 0.5% CMC-Na at an equal volume for 21 consecutive days. Tumor volumes were measured twice a week by vernier calipers and calculated using the formula $V \text{ (mm}^3\text{)} = 0.5 \times (\text{larger diameter} \times \text{smaller diameter}^2)$.

Following 21 days of Eth intervention, blood, tumors and spleen were collected, and stripped for cleaning and weighing. After that, the samples which had been frozen in liquid nitrogen were stored in a – 80 °C freezer.

ELISA assay

The blood was centrifuged at 3500 rpm for 15 min. Following this, the levels of vascular endothelial growth factors (VEGF), basic fibroblast growth factor (bFGF), interleukin 6 (IL-6), and tumor necrosis factor-α (TNF-α) in the serum were quantified using a commercially available ELISA assay kit (Elabscience Biotechnology Co., Ltd., China). Briefly, the corresponding standards were diluted in a gradient concentration, then 100 µL of standards and serum samples were added to a 96-well enzyme plate, and biotin anti-body, HRP conjugate, TMB substrate and stop solution were added sequentially according to the instruction manual of the reagent kit, and the optical density value at 450 nm was measured on anplate microplate reader (Tecan (Shanghai) laboratory equipment Co., Ltd., China). Finally, the final concentrations of VEGF, bFGF, IL-6 and TNF-α in serum were calculated from the standard curve established by the optical density value and concentration.

Quantitative real-time PCR analysis

Total RNA was obtained from tumor tissues and converted into cDNA using the cDNA kit according to the manufacturer's instructions (Servicebio, Wuhan). The SYBR Green kit (Servicebio, Wuhan) was used to analysis the gene expression. All primer sequences in Table 1 were synthesized by Wuhan Sangon Biotech. The $2^{-\Delta\Delta CT}$ method was used to analyse the data of the experiments using GAPDH as internal control.

Immunohistochemistry (IHC) staining

Immunohistochemistry was performed to assess the tumor tissue sections. The process involved dewaxing 4 µm sections in xylene for 5 min, followed by dehydration using 100%, 90%, and 70% of graded alcohols. Afterwards, antigen repair was conducted in citric acid antigen repair buffer. To block endogenous peroxidase, the sections were treated with 3% H₂O₂, and 3% BSA was added dropwise to evenly cover the tissue serum for serum blocking. The sections were incubated with primary antibodies (Ki67; E-Cadherin; N-Cadherin, 1:200, respectively), followed by biotin-conjugated secondary antibody. Immunoreactive membranes were visualized by an enhanced DAB kit (Abcam, UK). The intensity of staining of positive cells was observed under the microscope.

| Gene | Sense primer sequences5'-3' | Antisense primer sequences5'-3' |
|------------|-----------------------------|---------------------------------|
| GAPDH | CCTCGTCCCGTAGACAAAATG | TGAGGTCAATGAAGGGGTCGT |
| Ki67 | CTTGATGCTAAACCGAAAAGTGG | GTGATGGGCTCAGGTATGTCTC |
| E-Cadherin | ATGAAGGCGGGAATCGTG | CCGTAGAAACAGTAGGAGCAGC |
| N-Cadherin | ATGAAGGCGGGAATCGTG | CCGTAGAAACAGTAGGAGCAGC |

Table 1. The primer sequences of genes.

Western blot analysis

SW480 cells and tumor tissue in mice were lysed with RIPA lysis buffer (Servicebio, China) for 3 h. The supernatants were collected by centrifugation. 40 µg of protein was separated using 10% SDS-PAGE electrophoresis and transferred to a 0.22 µm polyvinylidene difluoride (PVDF) membrane. The membrane was blocked with skim milk powder solution, and the primary antibody was cultured in a shaking incubator at 4 °C overnight, and then washed with TBST. The secondary antibody combined with HRP diluted with blocking solution was cultured. Finally, BosterECL Star Western Blot assay (BOSTER, Wuhan, China) was used to detect the protein expression level.

Proteomics analysis

Serum samples underwent a series of procedures starting with depletion of high abundance proteins using the Protein Enrichment Small-Capacity Kit and the resulting eluate was collected. The eluate was then treated with acetone and incubated at – 20 °C for 2 h. The precipitate was dried using air and then reconstituted in a solution containing 8 M urea and 100 mM TEAB after the centrifugation process. The proteins in the samples were first treated with 10 mM DTT to reduce them, and then with 50 mM iodoacetamide (IAM) to alkylate them. The peptide samples underwent digestion with trypsin. Following this, the peptides were purified and dried, and ultimately analyzed using LC–MS/MS.

Approximately 200 ng peptides were separated on a reverse-phase C18 column at a flow rate of 0.3 µL/min at 50 °C. The mobile phases, A and B, were created using 0.1 percent formic acid in water and 0.1 percent formic acid in acetonitrile, respectively. The concentration of mobile phase B was incrementally adjusted from 2 to 22% over the initial 45 min, then increased to 35% over the subsequent 5 min, further raised to 80% over the following 5 min, and finally held at 80% for an additional 5 min.

Metabolomics analysis

The serum (50 µL) was thawed on ice, mixed with ice-cold methanol (150 µL) and whirled for 3min, followed by centrifugation for 10 min at 12,000 rpm 4 °C to collect the supernatants. Methods and processes in metabolomics are as described in previous studies in our lab on the technology⁷².

Statistical analysis

At least 6 independent tests were conducted, and the data were expressed as means ± standard deviation (SD) values. Student's t-test and one-way analysis of ANOVA using SPSS 25.0 software were used for comparisons between two groups and multiple groups. A P value of less than 0.05 was considered to be statistically significant. Raw data collected by UPLC-MS/MS were analyzed by Profile Analysis and SIMCA-P13.0 for principal component analysis (PCA) and orthogonal partial least squares discriminant analysis (OPLS-DA) to obtain the score map. Parameters with p-value less than 0.05 and VIP greater than 1.0 were set to identify potential markers. Databases such as Kyoto Encyclopedia of Genes and Genomes (KEGG), Human Metabolome Database (HMDB) and METLIN were used.

Data availability

The data that support the findings of this study are available from the corresponding author upon reasonable request.

Received: 22 March 2024; Accepted: 19 February 2025

Published online: 24 February 2025

References

1. Siegel, R. L., Miller, K. D. & Jemal, A. Cancer statistics, 2019. *CA Cancer J. Clin.* **69**, 7–34 (2019).
2. Keum, N. & Giovannucci, E. Global burden of colorectal cancer: Emerging trends, risk factors and prevention strategies. *Nat. Rev. Gastro Hepatol.* **16**, 713–732 (2019).
3. Hultcrantz, R. Aspects of colorectal cancer screening, methods, age and gender. *J. Intern. Med.* **289**, 493–507 (2021).
4. Hassan, M., Watari, H., AbuAlmaat, A., Ohba, Y. & Sakuragi, N. Apoptosis and molecular targeting therapy in cancer. *Biomed. Res. Int.* **2014**, 150845 (2014).
5. Matsuura, K., Canfield, K., Feng, W. & Kurokawa, M. Metabolic regulation of apoptosis in cancer. *Int. Rev. Cel Mol. Biol.* **327**, 43–87 (2016).
6. Wu, J. et al. Tannic acid repair of zearalenone-induced damage by regulating the death receptor and mitochondrial apoptosis signaling pathway in mice. *Environ. Pollut.* **287**, 117557 (2021).
7. Zhang, Y. et al. Regulation of TBBPA-induced oxidative stress on mitochondrial apoptosis in L02 cells through the Nrf2 signaling pathway. *Chemosphere* **226**, 463–471 (2019).

8. Wang, X. et al. Caffeic acid attenuates irradiation-induced hematopoietic stem cell apoptosis through inhibiting mitochondrial damage. *Exp. Cell Res.* **409**, 112934 (2021).
9. Bock, F. J. & Tait, S. W. G. Mitochondria as multifaceted regulators of cell death. *Nat. Rev. Mol. Cell Biol.* **21**, 85–100 (2020).
10. Wang, L. et al. Miltirone induced mitochondrial dysfunction and ROS-dependent apoptosis in colon cancer cells. *Life Sci.* **151**, 224–234 (2016).
11. Li, B. et al. Chaetoglobosin K induces apoptosis and G2 cell cycle arrest through p53-dependent pathway in cisplatin-resistant ovarian cancer cells. *Cancer Lett.* **356**, 418–433 (2015).
12. Wu, W. S., Chien, C. C., Liu, K. H., Chen, Y. C. & Chiu, W. T. Evodiamine prevents glioma growth, induces glioblastoma cell apoptosis and cell cycle arrest through jnk activation. *Am. J. Chin. Med.* **45**, 879–899 (2017).
13. Peng, Y., Wang, Y., Zhou, C., Mei, W. & Zeng, C. PI3K/Akt/mTOR pathway and its role in cancer therapeutics: are we making headway? *Front. Oncol.* **12**, 819128 (2022).
14. Fulda, S. Synthetic lethality by co-targeting mitochondrial apoptosis and PI3K/Akt/mTOR signaling. *Mitochondrion* **19**, 85–87 (2014).
15. Wang, B. & Li, J. Y. Piceatannol suppresses the proliferation and induced apoptosis of osteosarcoma cells through PI3K/AKT/mTOR pathway. *Cancer Manag. Res.* **12**, 2631–2640 (2020).
16. Linke, M., Fritsch, S. D., Sukhbaatar, N. & Weichhart, T. mTORC1 and mTORC2 as regulators of cell metabolism in immunity. *FEBS Lett.* **591**, 3089–3103 (2017).
17. Hoshii, T. et al. mTORC1 is essential for leukemia propagation but not stem cell self-renewal. *J. Clin. Investig.* **122**, 2114–2129 (2012).
18. Punt, C. J., Koopman, M. & Vermeulen, L. From tumour heterogeneity to advances in precision treatment of colorectal cancer. *Nat. Rev. Clin. Oncol.* **14**, 235–246 (2017).
19. Xu, W. et al. Alkaloids exhibit a meaningful function as anticancer agents by restraining cellular signaling pathways. *Mini-Rev. Med. Chem.* **22**, 968–983 (2022).
20. Kumar, S. & Agnihotri, N. Piperlongumine, a piper alkaloid targets Ras/PI3K/Akt/mTOR signaling axis to inhibit tumor cell growth and proliferation in DMH/DSS induced experimental colon cancer. *Biomed. Pharmacother.* **109**, 1462–1477 (2019).
21. Wei, W. J. et al. A review on classification and biological activities of alkaloids from the genus *Zanthoxylum* species. *Mini-Rev. Med. Chem.* **21**, 336–361 (2021).
22. Liu, H., Feng, J., Feng, K. & Lai, M. Optimization of the extraction conditions and quantification by RP-LC analysis of three alkaloids in *Zanthoxylum nitidum* roots. *Pharm. Biol.* **52**, 255–261 (2014).
23. An, D., Lin, Q. & Cheng, X. W. C. Investigation of the appropriateness of using ethoxychelerythrine as a representative quality marker of *Zanthoxylum nitidum*. *J. Planar Chromat.* **36**, 31–43 (2023).
24. Wang, P. et al. Necroptosis signaling and mitochondrial dysfunction cross-talking facilitate cell death mediated by chelerythrine in glioma. *Free Radic. Biol. Med.* **202**, 76–96 (2023).
25. Danielewski, M. et al. Sanguinarine-chelerythrine fraction of *Coptis chinensis* exerts anti-inflammatory activity in carrageenan paw oedema test in rats and reveals reduced gastrototoxicity. *Oxid. Med. Cell Longev.* **2022**, 1504929 (2022).
26. Bai, Y., Hou, J., Zhang, X. T., Gao, J. P. & Zhou, J. T. *Zanthoxylum bungeanum* seed oil elicits autophagy and apoptosis in human laryngeal tumor cells via PI3K/AKT/mTOR signaling pathway. *Anticancer Agents Med. Chem.* **21**, 2610–2619 (2021).
27. Qian, Y. et al. Integrating bioinformatics with pharmacological evaluation for illustrating the action mechanism of herbal formula Jiao'e mixture in suppressing lung carcinoma. *J. Ethnopharmacol.* **281**, 114513 (2021).
28. Alam, F., Najum Us Saqib, Q. & Waheed, A. Cytotoxic activity of extracts and crude saponins from *Zanthoxylum armatum* DC. against human breast (MCF-7, MDA-MB-468) and colorectal (Caco-2) cancer cell lines. *BMC Complement Altern. Med.* **17**, 368 (2017).
29. Chen, Z. J. et al. Hydroxy- γ -sanshool from *Zanthoxylum bungeanum* (prickly ash) induces apoptosis of human colorectal cancer cell by activating P53 and Caspase 8. *Front. Nutr.* **9**, 914638 (2022).
30. Ou, L. et al. Effects of cadmium on osteoblast cell line: Exportin 1 accumulation, p-JNK activation, DNA damage and cell apoptosis. *Ecotoxicol. Environ. Safe* **208**, 111668 (2021).
31. Childs, E. W., Tharakan, B., Hunter, F. A., Tinsley, J. H. & Cao, X. Apoptotic signaling induces hyperpermeability following hemorrhagic shock. *Am. J. Physiol. Heart C* **292**, H3179–H3189 (2007).
32. Shang, Y. et al. Zirconia nanoparticles induce hela cell death through mitochondrial apoptosis and autophagy pathways mediated by ROS. *Front. Chem.* **9**, 522708 (2021).
33. Yang, F. et al. LACTB induced apoptosis of oxaliplatin-resistant gastric cancer through regulating autophagy-mediated mitochondrial apoptosis pathway. *Am. J. Transl. Res.* **13**, 601–616 (2021).
34. Pistritto, G., Trisciuglio, D., Ceci, C., Garufi, A. & D'Orazi, G. Apoptosis as anticancer mechanism: Function and dysfunction of its modulators and targeted therapeutic strategies. *Aging* **8**, 603–619 (2016).
35. Khan, I. et al. Novel quercetin derivative TEF induces ER stress and mitochondria-mediated apoptosis in human colon cancer HCT-116 cells. *Biomed. Pharmacother.* **84**, 789–799 (2016).
36. Li, X. et al. The effect of caspase-3 in mitochondrial apoptosis activation on degradation of structure proteins of *Esox lucius* during postmortem storage. *Food Chem.* **367**, 130767 (2022).
37. Zhong, T. et al. 3, 3', 4, 4', 5-Pentachlorobiphenyl influences mitochondrial apoptosis pathway in granulosa cells. *J. Cell Biochem.* **120**, 15337–15346 (2019).
38. Lan, T., Zhao, H., Xiang, B., Wang, J. & Liu, Y. Suture compression induced midpalatal suture chondrocyte apoptosis with increased caspase-3, caspase-9, Bad, Bak, Bax and Bid expression. *Biochem. Biophys. Res. Commun.* **489**, 179–186 (2017).
39. Howells, C. C., Baumann, W. T., Samuels, D. C. & Finkielstein, C. V. The Bcl-2-associated death promoter (BAD) lowers the threshold at which the Bcl-2-interacting domain death agonist (BID) triggers mitochondria disintegration. *J. Theor. Biol.* **271**, 114–123 (2011).
40. Chen, X. et al. ST6Gal-I modulates docetaxel sensitivity in human hepatocarcinoma cells via the p38 MAPK/caspase pathway. *Oncotarget* **7**, 51955–51964 (2016).
41. Childs, B. G., Baker, D. J., Kirkland, J. L., Campisi, J. & van Deursen, J. M. Senescence and apoptosis: Dueling or complementary cell fates? *EMBO Rep.* **15**, 1139–1153 (2014).
42. Fridman, J. S. & Lowe, S. W. Control of apoptosis by p53. *Oncogene* **22**, 9030–9040 (2003).
43. Maraming, P. et al. Antitumor activity of RT2 peptide derived from crocodile leukocyte peptide on human colon cancer xenografts in nude mice. *Environ. Toxicol.* **33**, 972–977 (2018).
44. Bielenberg, D. R. & Zetterm, B. R. The contribution of angiogenesis to the process of metastasis. *Cancer J.* **21**, 267–273 (2015).
45. Zhao, M. et al. Expression of angiogenic growth factors VEGF, bFGF and ANG1 in colon cancer after bevacizumab treatment in vitro: A potential self-regulating mechanism. *Oncol. Rep.* **37**, 601–607 (2017).
46. Yang, L., Xiao, M., Li, X., Tang, Y. & Wang, Y. L. Arginine ADP-ribosyltransferase 1 promotes angiogenesis in colorectal cancer via the PI3K/Akt pathway. *Int. J. Mol. Med.* **37**, 734–742 (2016).
47. Tzeng, H. E., Chang, A. C., Tsai, C. H., Wang, S. W. & Tang, C. H. Basic fibroblast growth factor promotes VEGF-C-dependent lymphangiogenesis via inhibition of miR-381 in human chondrosarcoma cells. *Oncotarget* **7**, 38566–38578 (2016).
48. Maracle, C. X. et al. Silencing NIK potentiates anti-VEGF therapy in a novel 3D model of colorectal cancer angiogenesis. *Oncotarget* **9**, 28445–28455 (2018).

49. Lin, F. et al. USP43 promotes tumorigenesis through regulating cell cycle and EMT in breast cancer. *Int. J. Exp. Pathol.* **10**, 11014–11021 (2017).
50. Zhang, H. et al. Rhein suppresses colorectal cancer cell growth by inhibiting the mtor pathway in vitro and in vivo. *Cancers* **13**, 2176 (2021).
51. Shi, L. et al. SIRT5-mediated deacetylation of LDHB promotes autophagy and tumorigenesis in colorectal cancer. *Mol. Oncol.* **13**, 358–375 (2019).
52. Nagamine, A., Araki, T., Nagano, D., Miyazaki, M. & Yamamoto, K. L-Lactate dehydrogenase B may be a predictive marker for sensitivity to anti-EGFR monoclonal antibodies in colorectal cancer cell lines. *Oncol. Lett.* **17**, 4710–4716 (2019).
53. Ivancic, M. M. et al. Candidate serum biomarkers for early intestinal cancer using 15N metabolic labeling and quantitative proteomics in the ApcMin/+ mouse. *J. Proteome Res.* **12**, 4152–4166 (2013).
54. Altobelli, E., Marziani, D., Lattanzi, A. & Angeletti, P. M. Htr A1: Its future potential as a novel biomarker for cancer. *Oncol. Rep.* **34**, 555–566 (2015).
55. Zurawa-Janicka, D. et al. Expression of htra genes and its association with microsatellite instability and survival of patients with colorectal cancer. *Int. J. Mol. Sci.* **21**, 3947 (2020).
56. Du, S. et al. Prognostic and therapeutic significance of a novel ferroptosis related signature in colorectal cancer patients. *Bioengineered* **13**, 2498–2512 (2022).
57. Guo, W. et al. Self-assembly of a multifunction dna tetrahedron for effective delivery of aptamer PL1 and Pcsk9 siRNA potentiate immune checkpoint therapy for colorectal cancer. *ACS Appl. Mater. Int.* **14**, 31634–31644 (2022).
58. Liu, Z. et al. Potential targets identified in adenoid cystic carcinoma point out new directions for further research. *Am. J. Transl. Res.* **13**, 1085–1108 (2021).
59. Bao, Y. et al. 12N-Substituted matrinol derivatives inhibited the expression of fibrogenic genes via repressing Integrin/FAK/PI3K/Akt pathway in hepatic stellate cells. *Molecules* **24**, 3748 (2019).
60. Jin, R. et al. GPNMB silencing suppresses the proliferation and metastasis of osteosarcoma cells by blocking the PI3K/Akt/mTOR signaling pathway. *Oncol. Rep.* **39**, 3034–3040 (2018).
61. Brauns, S. C., Dealtry, G., Milne, P., Naudé, R. & Van de Venter, M. Caspase-3 activation and induction of PARP cleavage by cyclic dipeptide cyclo (Phe-Pro) in HT-29 cells. *Anticancer Res.* **25**, 4197–4202 (2005).
62. Yao, S. et al. Small molecule inhibition of CPS1 activity through an allosteric pocket. *Cell Chem. Biol.* **27**, 259–268 (2020).
63. Lee, Y. Y. et al. Overexpression of CPS1 is an independent negative prognosticator in rectal cancers receiving concurrent chemoradiotherapy. *Tumour Biol.* **35**, 11097–11105 (2014).
64. Nakamura, M., Manome, Y. & Ohno, T. Experimental gene therapy for colon carcinoma both in vitro and in vivo using a deoxycytidine kinase suicide gene together with cytosine arabinoside. *Jikeikai Med. J.* **49**, 173–181 (2002).
65. Fan, W., Zhou, Z. Y., Huang, X. F., Bao, C. D. & Du, F. Deoxycytidine kinase promotes the migration and invasion of fibroblast-like synoviocytes from rheumatoid arthritis patients. *Int. J. Exp. Pathol.* **6**, 2733–2744 (2013).
66. Peng, X. et al. 3, 6-Dihydroxyflavone suppresses breast carcinogenesis by epigenetically regulating miR-34a and miR-21. *Cancer Prev. Res.* **8**, 509–517 (2015).
67. Cao, Z. X. et al. Pogostone induces autophagy and apoptosis involving PI3K/Akt/mTOR axis in human colorectal carcinoma HCT116 cells. *J. Ethnopharmacol.* **202**, 20–27 (2017).
68. Siddiqui, A. & Ceppi, P. A non-proliferative role of pyrimidine metabolism in cancer. *Mol. Metab.* **3**, 5100962 (2020).
69. Wang, W., Cui, J., Ma, H., Lu, W. & Huang, J. Targeting pyrimidine metabolism in the Era of precision cancer medicine. *Front. Oncol.* **11**, 684961 (2021).
70. Tian, L. Y., Smit, D. J. & Jücker, M. The role of PI3K/AKT/mTOR signaling in hepatocellular carcinoma metabolism. *Int. J. Mol. Sci.* **24**, 2652 (2023).
71. Zha, X. et al. Lactate dehydrogenase B is critical for hyperactive mTOR-mediated tumorigenesis. *Cancer Res.* **71**, 13–18 (2011).
72. Si, Y. et al. Comprehensive 16S rDNA sequencing and LC-MS/MS-based metabolomics to investigate intestinal flora and metabolic profiles of the serum, hypothalamus and hippocampus in p-chlorophenylalanine-induced insomnia rats treated with *Lilium brownie*. *Neurochem. Res.* **47**, 574–589 (2022).

Author contributions

Conceptualization: Tao Guo, Weiwei Zhao and Shuying Feng; methodology: Yaqin Meng and Yanpo Si; software: Yaqin Meng and Yanpo Si; validation: Ke Sun; formal analysis: Yaqin Meng and Yanpo Si; investigation: Tao Guo and Shuying Feng; resources: Ke Sun; data curation: Yaqin Meng and Yanpo Si; writing—original draft preparation: Yaqin Meng and Yanpo Si; writing—review and editing: Tao Guo and Weiwei Zhao; visualization: Ya Wang; supervision: Lianping Wang; project administration: Liping Zhang; funding acquisition: Tao Guo. All authors have read and agreed to the published version of the manuscript.

Funding

This research was funded by the Henan Provincial High-Level Talents International Training funding project (2021-72), the Zhongjing Talent Backbone Project of Henan University of Chinese Medicine (00104311-2019-14).

Declarations

Competing interests

The authors declare no competing interests.

Ethical approval

The animal study protocol was approved by the Animal Ethics Committee of the Henan University of Chinese Medicine (protocol code DWLL202003253).

Additional information

Supplementary Information The online version contains supplementary material available at <https://doi.org/10.1038/s41598-025-91251-1>.

Correspondence and requests for materials should be addressed to T.G., W.Z. or S.F.

Reprints and permissions information is available at www.nature.com/reprints.

Publisher's note Springer Nature remains neutral with regard to jurisdictional claims in published maps and institutional affiliations.

Open Access This article is licensed under a Creative Commons Attribution-NonCommercial-NoDerivatives 4.0 International License, which permits any non-commercial use, sharing, distribution and reproduction in any medium or format, as long as you give appropriate credit to the original author(s) and the source, provide a link to the Creative Commons licence, and indicate if you modified the licensed material. You do not have permission under this licence to share adapted material derived from this article or parts of it. The images or other third party material in this article are included in the article's Creative Commons licence, unless indicated otherwise in a credit line to the material. If material is not included in the article's Creative Commons licence and your intended use is not permitted by statutory regulation or exceeds the permitted use, you will need to obtain permission directly from the copyright holder. To view a copy of this licence, visit <http://creativecommons.org/licenses/by-nc-nd/4.0/>.

© The Author(s) 2025